



1 **Last Interglacial climate and sea-level evolution from a**
2 **coupled ice sheet-climate model**

3 **H. Goelzer^{1*}, P. Huybrechts¹, Marie-France Loutre², Thierry Fichefet²**

4

5 ¹Earth System Sciences & Departement Geografie, Vrije Universiteit Brussel, Brussels,
6 Belgium

7 ²Université catholique de Louvain, Earth and Life Institute, Georges Lemaître Centre for
8 Earth and Climate Research (TECLIM), Louvain-la-Neuve, Belgium.

9 *now at: Institute for Marine and Atmospheric Research, Utrecht University, Utrecht, the
10 Netherlands

11 Correspondence to: H. Goelzer (heiko.goelzer@vub.ac.be)

12

13

14 **1 Abstract**

15 As the most recent warm period in Earth's history with a sea-level stand higher than present,
16 the Last Interglacial period (~130 to 115 kyr BP) is often considered a prime example to study
17 the impact of a warmer climate on the two polar ice sheets remaining today. Here we simulate
18 the Last Interglacial climate, ice sheet and sea-level evolution with the Earth system model of
19 intermediate complexity LOVECLIM v.1.3, which includes dynamic and fully-coupled
20 components representing the atmosphere, the ocean and sea ice, the terrestrial biosphere and
21 the Greenland and Antarctic ice sheets. In this set-up, sea-level evolution and climate-ice
22 sheet interactions are modelled in a consistent framework.

23 Surface mass balance changes are the dominant forcing for the Greenland ice sheet, which
24 shows a peak sea-level contribution of 1.4 m at 123 kyr BP in the reference experiment. Our
25 results indicate that ice sheet-climate feedbacks play an important role to amplify climate and
26 sea-level changes in the Northern Hemisphere. The sensitivity of the Greenland ice sheet to
27 surface temperature changes considerably increases when interactive albedo changes are
28 considered. Southern Hemisphere polar and sub-polar ocean warming is limited throughout



29 the Last Interglacial and surface and sub-shelf melting exerts only a minor control on the
30 Antarctic sea-level contribution with a peak of 4.4 m at 125 kyr BP. Retreat of the Antarctic
31 ice sheet at the onset of the LIG is mainly forced by rising sea-level and reduced ice shelf
32 viscosity as the surface temperature increases. Global sea level shows a peak of 5.3 m at
33 124.5 kyr BP, which includes a minor contribution of 0.35 m from oceanic thermal expansion.
34 Neither the individual contributions nor the total modelled sea-level stand show multi-
35 millennial time scale variations as indicated by some reconstructions.

36

37 **2 Introduction**

38 The climate and sea-level evolution of past warm periods in the history of the Earth can give
39 important insights into expected changes in the future. The Last Interglacial (LIG) in
40 particular is often considered as a prime candidate for a potential, albeit limited, analogue for
41 a warmer future world, due to a wealth of available reconstructions of climate and sea level
42 for this period ~130-115 thousand years (kyr) ago (e.g. Dutton et al., 2015). Problems for the
43 direct comparison between LIG and future climates arise mainly from the different forcing
44 responsible for the warming, which can be ascribed to orbital variations during the LIG and to
45 elevated levels of greenhouse gases in the future. During the LIG, global mean annual surface
46 temperature is thought to have been 1°C to 2°C higher and peak global annual sea surface
47 temperatures $0.7^{\circ}\text{C} \pm 0.6^{\circ}\text{C}$ higher than pre-industrial (e.g. Turney and Jones, 2010). Due to
48 polar amplification, high latitude surface temperatures, when averaged over several thousand
49 years, were at least 2°C larger than present (Masson-Delmotte et al., 2013) and were up to
50 5°C larger over the ice sheets (EPICA community members, 2004; Masson-Delmotte et al.,
51 2015). These high temperatures had severe consequences for the evolution of the ice sheets at
52 the onset and during the LIG as evidenced in large variations of sea level (Rohling et al.,
53 2014; Grant et al., 2012). Coming out of the penultimate glaciation with a sea-level
54 depression of up to 130 m, the global sea level has peaked during the LIG, estimated at 5.5 to
55 9 m higher than today (Dutton and Lambeck, 2012; Kopp et al., 2009; 2013), with a current
56 best estimate of 6 m above the present level (Masson-Delmotte et al., 2013).

57 A higher-than-present sea-level stand almost certainly implies a complete melting of the
58 Laurentide and Fennoscandian ice sheets and a contribution from the Greenland ice sheet
59 (GrIS), from the Antarctic ice sheet (AIS) or from both. However, ice sheet retreat should not
60 be assumed synchronous in the Northern and Southern hemispheres and between individual



61 ice sheets. Fluctuations in global sea-level during the LIG period (Thompson et al., 2011,
62 Kopp et al., 2013) could be a consequence of differences in the timing of retreat and regrowth
63 e.g. between the Greenland and Antarctic ice sheets.

64 Because thus far direct evidence for an Antarctic ice sheet contribution to the LIG sea-level
65 high-stand is elusive, support for a contribution from the AIS is usually given as a residual of
66 total sea-level stand minus contributions from the GrIS, thermal expansion (THXP) and
67 glaciers and small ice caps (GIIC). This illustrates that the attribution problem is so far largely
68 underdetermined. It appears that the lower bound of 5.5 m (Dutton and Lambeck, 2012; Kopp
69 et al., 2013) could be fully explained by maximum values given in the IPCC AR5 (Masson-
70 Delmotte et al., 2013) for the contributions of the GrIS (1.4 - 4.3 m), GIIC (0.42 ± 0.11 m)
71 and THXP (0.4 ± 0.3 m) combined. However, assuming central estimates for all individual
72 components and the total would indicate an Antarctic contribution of ~ 3 m, which would be
73 in line with the contribution estimated for a collapse of the West Antarctic ice sheet (WAIS)
74 alone (Bamber et al., 2009). An Antarctic component is generally assumed to have foremost
75 come from the WAIS, which is thought to be vulnerable due to its marine-based character. It
76 is often speculated to be sensitive to ocean warming and increased sub-shelf melting (e.g.
77 Duplessy et al., 2007; Holden et al., 2010), caused by the interhemispheric see-saw effect
78 (Stocker, 1998). However, a combination of partial WAIS collapse and some East Antarctic
79 ice sheet (EAIS) retreat is also a possibility due to the large size of the latter. High-end
80 estimates of sea-level change can only be reconciled with an additional East Antarctic ice
81 sheet contribution, supposedly from marine-based sectors in the Wilkes and Aurora basins
82 (Pollard and DeConto, 2015). One issue complicating the residual argument is the
83 aforementioned possibility of different timing of the GrIS and AIS contributions. Indirect
84 evidence of a WAIS reduction or collapse may come from climate modelling studies that
85 attempt to explain stable-isotope ratios from ice (core) records (Holden et al., 2010, Steig et
86 al., 2015).

87 The Greenland ice sheet evolution is somewhat better constrained by ice core records both in
88 the central part (GRIP, NGRIP, NEEM) and at the periphery (Dye-3, Camp Century), even if
89 interpretation of the lower parts of the records remain ambiguous. To this date, none of the
90 Greenland ice cores shows continuous and undisturbed information back in time through the
91 LIG and into the penultimate glacial maximum. The relatively high temperatures during the
92 LIG as reconstructed from the folded lower parts of the NEEM ice core (NEEM community



93 members, 2013) seem to be incompatible with the general view that the ice sheet has lost
94 rather little volume during the LIG (e.g. Robinson et al., 2011; Colville et al., 2011; Rybak
95 and Huybrechts, in prep.). Several studies have therefore attempted to identify possible biases
96 in the NEEM reconstructions (e.g. van De Berg et al., 2013; Merz et al., 2014; Sjolte et al.,
97 2014; Steen-Larsen et al., 2014, Masson-Delmotte et al., 2015). Furthermore, the minimum
98 extent and margin position of the northeastern part of the ice sheet is not well constrained,
99 leaving room for alternative retreat scenarios (e.g. Born et al., 2012).

100 Modelling studies of the Greenland ice sheet for the entire LIG period so far often use
101 parameterised representations of the climate forcing (e.g. Huybrechts, 2002) or forcing based
102 on time slice climate experiments (e.g. Born et al., 2012; Stone et al., 2013), while full
103 coupling between ice and climate models is still a challenge and limited to models of
104 intermediate complexity (e.g. Robinson et al., 2011). Ice sheet modelling studies with specific
105 focus on the Antarctic ice sheet during the LIG are rare due to the aforementioned lack of
106 climate and geomorphological constraints for that period. However, results have been
107 presented in studies with focus on other time periods (e.g. Huybrechts, 2002) or with interest
108 on longer time scales (e.g. Pollard and deConto, 2009; de Boer et al., 2013, 2014).

109 The fundamental shortcoming at present for improving modelled constraints on the LIG ice
110 sheet contribution to sea level with physical models is the sparse information on LIG polar
111 climate and oceanic conditions over the ice sheets and in their proximity. Consequently, our
112 effort is directed towards studying key mechanisms and feedback processes in the coupled
113 climate-ice sheet system during the LIG. Here, we present modelling results from high
114 resolution ice sheet models of the Greenland and Antarctic ice sheets fully coupled to a
115 climate model of intermediate complexity run for the time period 135 kyr BP to 115 kyr BP.
116 In this set-up LIG sea-level evolution and climate-ice sheet interactions can be modelled in a
117 consistent framework. In the following, we describe the model (section 3) and the
118 experimental setup (section 4) and present results (section 5) and conclusions (section 6).

119

120 **3 Model description**

121 We use the Earth System Model of Intermediate Complexity (EMIC) LOVECLIM version
122 1.3, which includes components representing the atmosphere, the ocean and sea ice, the
123 terrestrial biosphere and the Greenland and Antarctic ice sheets (Figure 1). The model has
124 been utilised in a large number of coupled climate-ice sheet studies (e.g. Driesschaert et al.,



125 2007; Swingedouw et al., 2008; Goelzer et al., 2011; 2012a). Version 1.2 is described in
126 detail in Goosse et al. (2010). The present set-up of the climate model component is identical
127 to the model used in Loutre et al. (2014) and Goelzer et al. (2015). Where in the latter study
128 the ice sheet components were prescribed and used as forcing for the climate model, in the
129 present work, they are fully two-way coupled with information exchanged every full year.
130 The model components for the Greenland and Antarctic ice sheets are three-dimensional
131 thermomechanical ice-dynamic models (Huybrechts and de Wolde, 1999), which have been
132 utilised for long-term stand-alone ice sheet simulations in the past (Huybrechts, 2002).

133 Because of the relatively coarse resolution of the atmosphere in LOVECLIM (T21), the high-
134 resolution ice sheet models (10x10 km for Greenland and 20x20 km for Antarctica) are forced
135 with temperature anomalies and precipitation ratios relative to the pre-industrial reference
136 climate. The ice sheet models in turn provide the climate model with changing topography,
137 ice sheet extent (albedo) and spatially and temporally variable freshwater fluxes, unmodified
138 to earlier versions of the model (Goosse et al., 2010). Recent model improvements for the ice-
139 climate coupling interface are described in Appendix A.

140 **3.1 Northern Hemisphere ice sheet forcing**

141 At the onset of the LIG, large Northern Hemisphere (NH) ice sheets other than on Greenland
142 were still present and melted away over the course of several millennia. To account for these
143 ice sheet changes and their impact on climate and ocean evolution, a reconstruction of the
144 penultimate deglaciation of the NH is necessary for our experiments starting in 135 kyr BP.
145 Because there is very little geomorphological evidence for NH ice sheet constraints during
146 Termination II, a reconstruction of NH ice sheet evolution is made by remapping the retreat
147 after the last glacial maximum according to the global ice volume reconstruction (Lisiecki and
148 Raymo, 2005) during the onset of the LIG. The same procedure was already used in earlier
149 work to produce NH ice sheet boundary conditions for climate model simulations (Loutre et
150 al., 2014; Goelzer et al., 2015).

151 **3.2 Modelled sea-level change**

152 The modelled sea-level evolution takes into account contributions from the prescribed NH ice
153 sheets, the Greenland and Antarctic ice sheets and the steric contribution due to density
154 changes of the ocean water. The only component not explicitly modelled is the contribution of



155 glaciers and small ice caps, which have been estimated to give a maximum contribution of
156 0.42 ± 0.11 m during the LIG (Masson-Delmotte et al., 2013) and may contain as much as 5-
157 6 m SLE during glacial times (CLIMAP, 1981; Clark et al., 2001).

158 The Antarctic contribution to global sea-level change is calculated taking into account
159 corrections for ice replacing and being replaced by seawater *and* seawater being replaced by
160 isostatic bedrock movement, both mainly of importance for the marine sectors of the WAIS.
161 Note that this effect is not considered in the climate model, which operates with a fixed
162 present-day land-sea mask. The additional correction for bedrock changes is responsible for a
163 ~ 3 m lower sea-level contribution at 135 kyr BP compared to taking only changes in volume
164 above floatation into account. This additional sea-level depression arises from depressed
165 bedrock under the load of the ice in the marine sectors of the ice sheet.

166 For the Greenland ice sheet, the same corrections are applied, where the marine extent of ice
167 grounded below sea level is parameterised. However, the corrections imply only a ~ 30 cm
168 lower contrast to present day sea level due to Greenland ice sheet expansion at 135 kyr BP
169 and ~ 15 cm higher at 130 kyr BP compared to calculations based on the entire grounded ice
170 volume. The change in sign arises from bedrock changes in delayed response to ice loading
171 changes.

172 The steric component of global sea level considers density changes due to local changes of
173 temperature and salinity, but global salinity is restored as often done in ocean models to
174 guarantee stability.

175

176 **4 Experimental setup**

177 **4.1 Model forcing**

178 All simulations are forced by time-dependent changes in greenhouse gas (GHG)
179 concentrations and insolation running from 135 kyr BP until 115 kyr BP (Figure 2). The
180 radiative forcing associated with the reconstructed GHG levels is below preindustrial values
181 for most of this period and hardly exceeds it at ~ 128 kyr BP. The changes in the distribution
182 of insolation received by the Earth are dynamically computed from the changes in the orbital
183 configuration (Berger, 1978) and represent the governing forcing during peak LIG conditions.



184 In order to account for coastline changes and induced grounding line changes, both ice sheet
185 models are forced by changes in global sea-level stand (Figure 2c) using a recent sea-level
186 reconstruction based on Red Sea data (Grant et al., 2012). The chronology of the latter
187 assumes ice volume to be independent of deep-sea temperatures, in contrast to directly using
188 the scaled benthic $\delta^{18}\text{O}$ record as sea-level proxy (Shakun et al., 2015). In this sea-level
189 forcing approach, local changes due to geoidal eustasy are not taken into account, which
190 would result in lower amplitude sea-level changes close to the ice sheets, but would not be
191 consistent with the stand-alone spin-up of the ice sheet models.

192 As mentioned earlier, the ice sheet models are forced with temperature anomalies relative to
193 the pre-industrial reference climate. As a measure to ensure a realistic simulation of the
194 Greenland ice sheet evolution, the temperature anomaly forcing from the climate model over
195 the Greenland ice sheet needs to be rescaled. In absence of such scaling, the ice sheet almost
196 completely melts away over the course of the LIG in disagreement with the ice core data,
197 which suggests a large remaining ice sheet during the LIG (Dansgaard et al., 1982; NEEM
198 community members, 2013). In the absence of firm constraints on climate evolution over the
199 ice sheet, the temperature scaling in the present study represents a pragmatic solution to
200 produce an ice sheet evolution reasonably in line with ice core constraints on minimum ice
201 sheet extent during the LIG. A uniform scaling of the atmospheric temperature anomaly with
202 a factor of $R=0.4$ was adopted in the reference experiment and is later compared to two
203 sensitivity experiments with modified scaling ($R=0.5, 0.3$).

204 The fully coupled experiments are accompanied by additional sensitivity experiments, in
205 which the ice sheet models are forced in stand-alone mode with (modified) climate forcing
206 produced by the fully coupled runs. These experiments serve to study ice sheet sensitivity in
207 response to changes in the climate forcing and are also used to evaluate ice sheet-climate
208 feedbacks in comparison between the coupled and un-coupled system. The ice sheet response
209 in the reference stand-alone experiment (forced offline with the recorded climate forcing of
210 the coupled reference run) is by construction identical to the response in the fully coupled run.
211 Additional experiments have been run with modified temperature scaling for the Greenland
212 ice sheet ($R=0.5, 0.3$), which can be compared to the respective fully coupled experiment. For
213 the AIS, experiments with suppressed shelf melting have been performed to isolate the effect
214 of ocean temperature changes on the ice volume evolution and sea-level contribution.



215 **4.2 Initialisation**

216 The goal of our initialisation technique is to prepare a coupled ice sheet-climate model state
217 for the transient simulations starting at 135 kyr BP exhibiting a minimal coupling drift. Both
218 ice sheet models are first integrated over the preceding glacial cycles in order to carry the
219 long-term thermal and geometric history with them. The climate model is then initialized to a
220 steady state with ice sheet boundary conditions, greenhouse gas forcing and orbital
221 parameters for the time of coupling (135 kyr BP). When LOVECLIM is integrated forward in
222 time in fully coupled mode, the climate component is already relaxed to the ice sheet
223 boundary conditions. The mismatch between stand-alone ice sheet forcing and climate model
224 forcing is incrementally adjusted in the period 135-130 kyr BP with a linear blend between
225 the two to minimize the effect of changing boundary conditions for the ice sheet model. A
226 small, unavoidable coupling drift of the ice sheet component arises from a switch of spatially
227 constant to spatially variable temperature and precipitation anomalies at the time of coupling,
228 but is uncritical to the results.

229

230 **5 Results**

231 The modelled LIG climate evolution and comparison with reconstructions were presented in
232 detail in two earlier publications (Loutre et al., 2014; Goelzer et al., 2015) for the same
233 climate model setup. Differences to the work by Goelzer et al. (2015) arise from a different
234 ice sheet evolution and feedbacks between climate and ice sheets that are taken into account
235 in our present, fully coupled approach.

236 Global annual mean near-surface air temperature in the reference experiment shows a distinct
237 increase until 129 kyr BP in response to orbital and greenhouse gas forcing and to an even
238 larger extent in response to changes in ice sheet boundary conditions (Figure 3). The peak
239 warming reaches 0.3 °C above the pre-industrial at 125.5 kyr BP. Thereafter, cooling sets in
240 and continues at a much lower rate compared to the rate of warming before 129 kyr BP. The
241 importance of ice sheet changes is illustrated by comparing the reference experiment with a
242 climate simulation (Loutre et al., 2014) forced by insolation and GHG changes only (noIS)
243 and with a one-way coupled climate model run (Goelzer et al., 2015) forced with prescribed
244 NH, Antarctic and Greenland ice sheet changes (one-way). The much larger temperature
245 contrast at the onset of the LIG compared to noIS arises from changes in surface albedo and
246 melt water fluxes of the Northern Hemisphere ice sheets, which freshen the North Atlantic



247 and lead to a strong reduction of the Atlantic meridional overturning circulation. The episode
248 of relative cooling in the reference experiment with a local temperature minimum at 128 kyr
249 BP is due to cooling of the Southern Ocean (SO and sea-ice expansion in response to large
250 Antarctic freshwater fluxes caused mainly by the retreat of the WAIS, which occurs 2 kyr
251 later compared to the one-way experiment.

252 **5.1 Greenland ice sheet**

253 The Greenland ice sheet evolution over the LIG period is largely controlled by changes in the
254 surface mass balance with predominant importance of the ablation (Figure 4). Marginal
255 summer surface melt water runoff is the dominant mass loss of the ice sheet after 130 kyr BP,
256 when the ice sheet has retreated largely on land. Due to increased temperatures over
257 Greenland, the mean accumulation rate (averaged over the ice covered area) is consistently
258 above the present-day reference level after 128 kyr BP, but increases to at most 18% higher.
259 Conversely, the mean ablation rate over Greenland shows an up to threefold increase
260 compared to the present day with consistently higher-than present rates between 130.5 kyr to
261 120.5 kyr BP. Temperature anomalies responsible for the increased ablation are on average
262 above zero between 129.5 kyr to 120.5 kyr BP and peak at 1.3 °C (after scaling) around 125
263 kyr BP. The calving flux decreases as the ice sheet retreats from the coast (in line with
264 decreasing area and volume, Figure 5) and as surface melting and runoff increase, removing
265 some of the ice before it can reach the coast. In the second half of the experiment, runoff
266 decreases with decreasing temperature anomalies and the calving flux increases again with
267 increasing ice area and volume.

268 Entering the warm period, the furthest retreat of the ice sheet occurs in the southwest and
269 northwest (Figure 5), accompanied by an overall retreat from the coast. Conversely, the ice
270 sheet gains in surface elevation over the central dome due to increased accumulation. By 115
271 kyr BP, the ice sheet has regrown beyond its present day area almost everywhere and contact
272 with the ocean is increasing. The GrIS volume change translates into a sea-level contribution
273 peak of 1.4 m at 123 kyr BP (Figure 9). For the two sensitivity experiments (high, low) with
274 modified scaling ($R=0.5, 0.3$), the contribution changes to 2.8 m and 0.6 m, respectively.

275 NEEM ice core data (NEEM community members, 2013) and radiostratigraphy of the entire
276 ice sheet (MacGregor et al., 2015) indicate that the NEEM ice core site was ice covered
277 through the entire Eemian as is the case for our reference experiment. Elevation changes from



278 that ice core are however not well constrained and leaves room for a wide range of possible
279 retreat patterns of the northern GrIS (e.g. Born et al., 2012). The Camp Century ice core
280 record contains some ice in the lowest part with a colder signature than ice dated as belonging
281 to the Eemian period (Dansgaard et al., 1982). It is likely that this ice is from before the
282 Eemian even in view of possible disturbance of the lower levels, which was shown to exist for
283 the NEEM core site (NEEM community members, 2013). Reconstruction of the age structure
284 from radiostratigraphy (MacGregor et al., 2015) shows no ice at the Camp Century location
285 before 115 kyr BP. However, it is possible that isochrones were disturbed and unreliable for
286 interpretation in this region. In view of this evidence, the north-western retreat of the ice sheet
287 in our reference simulation may be too far, a direct result of the largely unconstrained climatic
288 forcing. It was shown that a different climate forcing could produce e.g. a larger northern
289 retreat still in line with the (limited) paleo evidence (Born et al., 2012). Some more thinning
290 and retreat in the south is also possible without violating constraints on minimal ice sheet
291 extent from Dye-3 (Dansgaard et al., 1982). LIG ice cover of the Dye-3 site is not a necessity
292 when taking into consideration that older ice found at the base of the core could have flowed
293 in from a higher elevation.

294 The climatic temperature anomaly over central Greenland in the coupled model shows a flat
295 maximum around 127 kyr BP, similar to the global temperature evolution, but 2 kyr earlier
296 compared to the NEEM reconstructions (NEEM community members, 2013). If assuming
297 present-day configuration and spatially constant warming, ice mass loss from the GrIS could
298 be expected to occur approximately as long as the temperature anomaly remains above zero,
299 which is the case until ~ 122 kyr BP in the model and until ~ 119 kyr BP in the NEEM
300 reconstruction. With a lower surface elevation, the time the ice sheet starts to gain mass again
301 would be further delayed. Even with considerable uncertainty due to uncertain spatial pattern
302 of the warming, which modifies this simple reasoning, we argue that the peak sea-level
303 contribution from the GrIS has to occur late during the LIG. Based on the same argument,
304 there is no evidence in the reconstructed NEEM temperature evolution suggesting a regrowth
305 or substantial pause of melting of the Greenland ice sheet any time during the LIG.

306 The need for scaling the temperature forcing to produce a realistic Greenland ice sheet
307 evolution equally applies when forcing our stand-alone ice sheet model with the temperature
308 reconstructed from the NEEM ice core record (NEEM community members, 2013). It appears
309 that practically any ice sheet model with (melt parameters tuned for the present day) would



310 project a near-complete GrIS meltdown, if the amplitude and duration of warming suggested
311 by the NEEM reconstructions would apply for the entire ice sheet. This problem would be
312 further amplified if insolation changes were explicitly taken into account in the melt model
313 (Robinson and Goelzer, 2014). We refer to this mismatch between reconstructed temperatures
314 and assumed minimum ice sheet extent as the “NEEM paradox”. Several attempts to solve
315 this paradox have been made by suggesting possible biases in the interpretation of the
316 relationship between isotope ratio and temperature, which may not be assumed temporally
317 and spatially constant (e.g. Merz et al., 2014; Sjolte et al., 2014; Steen-Larsen et al., 2014,
318 Masson-Delmotte et al., 2015) and may be affected by changes in the precipitation regime
319 (van De Berg et al., 2013). From the modelling point of view, the decisive question is over
320 what spatial extent and when during the year the temperature reconstruction (and possible
321 future reinterpretations) for the NEEM site should be assumed. A central Greenland warming
322 of large magnitude could only be reconciled with the given geometric constraints if a (much)
323 lower warming was present over the margins and during the summer, which is where and
324 when the majority of the mass loss due to surface melting is taking place.

325 The strength of the ice-climate feedback on Greenland was examined by comparing additional
326 experiments in which the coupling between ice sheet and climate is modified. Results from
327 the fully coupled model (Reference) are compared to those from forced ice sheet runs (SA),
328 which are driven with the climate forcing from the coupled reference model run. In both cases
329 the scaling of Greenland forcing temperature is set to a magnitude of 0.3 (low), 0.4 (ref) and
330 0.5 (high), respectively. When the feedback between ice sheet changes and climate is included
331 in the coupled experiments, the warming over the margins is considerably increased (reduced)
332 for experiment high (low) compared to the stand-alone experiments. Consequently, sea-level
333 contributions show a non-linear dependence on the temperature scaling for the fully coupled
334 run, while they are near linear for the forced runs (Figure 6, left). The dominant feedback
335 mechanism arises from how changing albedo characteristics are taken into account for a
336 melting ice sheet surface. The albedo can change due to changes in snow depth and also due
337 to changes of the snow cover fraction, which indicates how much surface area of a grid cell is
338 covered with snow (Figure 6, right). Both lead to lower albedo and increased temperatures in
339 places where the ice sheet starts melting at the surface. The difference in warming between
340 stand-alone and fully-coupled experiments is therefore located over the ice sheet margins and
341 does not have a considerable influence on the NH or global temperature response. The albedo
342 effects are near-instantaneous and their importance for the ice sheet response underline earlier



343 findings that a basic albedo treatment is an essential aspect of a coupled ice–climate
344 modelling system (e.g. Robinson and Goelzer, 2014). A third, but comparatively smaller
345 effect arises from the retreating ice sheet margin being replaced by lower albedo tundra
346 (Figure 6, right), which operates on much longer time scales.

347

348 **5.2 Antarctic ice sheet**

349 The annual mean air temperature anomaly over Antarctica (averaged over grounded ice)
350 increases at the beginning of the experiment to a peak at 125 kyr BP (Figure 7), before
351 cooling sets in and continues until 115 kyr BP. The warming necessary to reach temperature
352 anomalies of up to two degrees is around a factor two faster than the cooling trend afterwards,
353 with both transitions being near linear on the millennial time scale. The Antarctic ice sheet
354 surface climate appears to be largely isolated from millennial time scale perturbations
355 occurring in the Southern Ocean in response to changing freshwater fluxes in both
356 hemispheres. While freshwater fluxes from the retreating Antarctic ice sheet itself lead to sea-
357 ice expansion and surface cooling in the Southern Ocean, freshwater fluxes from the decay of
358 the Northern Hemisphere ice sheets are communicated to the SH by the interhemispheric see-
359 saw effect (Goelzer et al., 2015). Pre-industrial surface temperature levels are first reached
360 128 kyr BP and after cooling again at 118 kyr BP. The accumulation rate (averaged over
361 grounded ice) shows an initial increase in line with the higher temperatures until 130 kyr BP
362 but records a changing grounded ice sheet area further on, which mostly indicates retreat of
363 the ice sheet from regions of higher accumulation. Relative to the pre-industrial, accumulation
364 increases at most 20 % in annual values and up to 12 % for the long-term mean (grey and
365 black lines in Figure 7, respectively). As a consequence of the surface forcing, the AIS shows
366 a small volume gain until 130.5 kyr BP due to increase in precipitation before a large-scale
367 retreat of the grounding line sets in. The average ablation rate over grounded ice equally
368 increases with increasing temperature but remains of negligible importance for the mass
369 balance of the ice sheet (note difference of vertical scales between panel b and c in Figure 7).

370 Changes in the sub-shelf melt rate play an important role for the present mass balance of the
371 AIS and are often discussed as a potential forcing for a WAIS retreat during the LIG (e.g.
372 Duplessy et al., 2007; Holden et al., 2010) and during the last deglaciation (Golledge et al.,
373 2014). The average sub-shelf melt rate diagnosed for the area of the present-day observed ice



374 shelves in our reference simulation increases to at most 20 % above the pre-industrial with a
375 peak in line with the air temperature maximum. However, ocean warming to above pre-
376 industrial temperatures occurs already before 130 kyr BP, more than 2 kyr earlier compared to
377 the air temperature signal. This is a consequence of the interhemispheric see-saw effect
378 (Stocker, 1998), which explains SO warming and cooling in the North Atlantic as a
379 consequence of reduced oceanic northward heat transport due to weakening of the Atlantic
380 meridional overturning circulation.

381 Ice sheet area and volume decrease rapidly between 129 and 127 kyr BP, and indicate a
382 gradual regrowth after 125 kyr BP. Those changes arise mainly from a retreat and re-advance
383 of the WAIS (Figure 8). In our model, the retreat exhibits characteristics of an overshoot
384 behaviour due to the interplay between ice sheet retreat and bedrock adjustment. The rebound
385 of the bedrock, which is initially depressed under the glacial ice load, is delayed compared to
386 the relatively rapid ice sheet retreat, giving rise to a grounding-line retreat well beyond the
387 pre-industrial steady-state situation. These results are in line with earlier work with a stand-
388 alone ice sheet model (Huybrechts, 2002), but also rely on a relatively large glacial-
389 interglacial loading contrast in these particular models. The sea-level contribution above the
390 present-day level from the Antarctic ice sheet peaks at 125 kyr BP at 4.4 m.

391 Stand-alone sensitivity experiments, in which specific forcing processes are suppressed, show
392 that surface melting and sub-shelf melting play a limited role for the AIS retreat in our
393 experiments. The sea-level contribution peak in an experiment with suppressed sub-shelf
394 melting is about 40 cm lower compared to the reference experiment and remains around one
395 meter lower between 123 kyr BP until the end of the experiment. The difference between the
396 experiments at a given point in time arises from a lower overall sea-level contribution when
397 sub-shelf melting is suppressed, but also from a difference in timing between both cases. The
398 dominant forcing for the Antarctic ice sheet retreat in our model is a combination of rising
399 global sea level and increasing surface temperature, which leads to increasing buoyancy and
400 reduced ice shelf viscosity, respectively. The relative timing between sea-level forcing and
401 temperature forcing is therefore of critical importance for the evolution of the ice sheet at the
402 onset of the LIG.

403 The limited effect of surface melting and sub-shelf melting on the sea-level contribution is
404 ultimately due to a limited magnitude of surface temperature and ocean temperature changes.
405 The limited Antarctic and SO temperature response has already been highlighted in earlier



406 studies with the same climate component (Loutre et al., 2014; Goelzer et al., 2015) and is
407 confirmed here with a fully-coupled model. The feedback mechanism suggested by Golledge
408 et al. (2014) for Termination I, which draws additional heat for sub-shelf melting from
409 freshwater-induced SO stratification and sea-ice expansion is active in our experiment, but
410 too short-lived and of too little amplitude to lead to substantially increased melt rates. Our
411 limited AIS response to environmental forcing is also in line with other modelling results for
412 the LIG period (Pollard and DeConto, 2015) albeit with a different forcing strategy, where
413 substantial retreat of marine based sectors of the EAIS can only be achieved by including
414 special treatment of calving fronts and shelf melting, which was not attempted here.

415 As mentioned earlier, direct constraints of the Antarctic ice sheet configuration during the
416 LIG are still lacking. Goelzer et al. (2015) suggested that the timing of the main glacial-
417 interglacial retreat of the AIS could be constrained by a freshwater induced oceanic cold event
418 recorded in ocean sediment cores (Bianchi and Gersonde et al. 2002). The main retreat in their
419 model happened ~129.5 kyr BP, a timing predating the time of retreat in the coupled model
420 by ~2 kyr due to the difference in atmospheric and oceanic forcing. It is noteworthy in this
421 context that the prescribed sea-level forcing imposes an important control for the timing of the
422 Antarctic retreat. Sensitivity experiments indicate that the main retreat appears another 2 kyr
423 later when a sea-level forcing based on a benthic $\delta^{18}\text{O}$ record (Lisiecki and Raymo, 2005) is
424 used instead of the sea-level reconstruction of Grant et al. (2012).

425 **5.3 Thermal expansion of the ocean**

426 The steric sea-level component due to ocean thermal expansion (Figure 9c) is largely
427 following the global temperature evolution, but is also strongly modified by changes in ice
428 sheet freshwater input. Ocean expansion is steep during peak input of freshwater and stagnant
429 during episodes of decreasing freshwater input. This is because the net ocean heat uptake is
430 large when freshwater input peaks, which happens in three main episodes in our experiment.
431 Two episodes of freshwater input from the NH centred at 133.6 and 131.4 kyr BP are
432 followed by an episode of combined input from the NH and the AIS centred at 128.2 kyr BP
433 (not shown). The anomalous freshwater input leads to stratification of the surface ocean, sea-
434 ice expansion and reduction of the air-sea heat exchange, effectively limiting the ocean heat
435 loss to the atmosphere. This implies that global sea-level rise due to ice sheet melting is
436 (weakly and temporarily) amplified by the freshwater impact on ocean thermal expansion. We
437 simulate a peak sea-level contribution from thermal expansion of 0.35 m at 125.4 kyr BP,



438 which forms part of a plateau of high contribution between 127.3 and 124.9 kyr BP (Figure
439 9c). The amplitude is at the lower end, but well within the range of IPCC AR5 estimates of
440 0.42 ± 0.11 m (Masson-Delmotte et al., 2013).

441

442 **5.4 Global sea-level change**

443 Combining contributions from GrIS, AIS, thermal expansion, global sea level peaks at ~ 5.3 m
444 at 124.5 kyr BP with a slow decrease thereafter as first the Antarctic ice sheet and 2 kyr later
445 the Greenland ice sheet start to regrow. For the Antarctic ice sheet the model indicates a clear
446 asymmetry between relatively fast retreat and much slower regrowth.

447 Modelled GrIS and AIS sea-level contributions together with prescribed NH sea level are
448 within the 67% confidence interval of probabilistic sea-level reconstructions (Kopp et al.,
449 2009) for the period ~ 125 -115 kyr BP (Figure 10). The last 20 m rise in sea-level
450 contributions from the NH (including Greenland) is steeper and occurs 1-2 kyr earlier in our
451 model compared to what the reconstructions suggest, which is consequently also the case for
452 the rise in global sea level at the onset of the LIG. The Antarctic retreat in our model is more
453 rapid compared to the reconstruction and does not show the hiatus ~ 131 -129 kyr BP
454 suggested by the data. The modelled ice sheet evolution in our reference run reproduces well
455 the global average sea-level contribution 125-115 kyr BP based on the best estimate of Kopp
456 et al. (2009) when taking into account the modelled steric contribution (0.35 m) and assuming
457 an additional contribution (0.42 ± 0.11 m) of glaciers and small ice caps (Masson-Delmotte et
458 al., 2013). The multi-peak structure of global sea-level contributions during the LIG
459 suggested by the reconstructions (Kopp et al., 2009; 2013) is not reproduced with our model,
460 mainly owing to the long response times of the ice sheets during regrowth to changing
461 climatic boundary conditions.

462

463 **6 Conclusion**

464 We have presented a coupled transient simulation of the entire LIG period with interactive
465 Greenland and Antarctic ice sheet components. In our results, both ice sheets contribute to the
466 sea-level high stand during the Last Interglacial, but are subject to different forcing and
467 response mechanisms. While the GrIS is mainly controlled by changes in surface melt water



468 runoff, the Antarctic ice sheet is only weakly affected by surface and sub-shelf melting.
469 Instead, grounding line retreat of the AIS is forced by changes in sea level stand and surface
470 warming, which lowers the shelf viscosity. Limited by the existing ice core constraints on
471 minimal ice sheet extent, the peak Greenland ice sheet contribution in our reference
472 experiment is 1.4 m, while the Antarctic contribution is 4.4 m predominantly sourced from
473 WAIS retreat. The modelled steric contribution is 0.35 m, in line with other modelling
474 studies. Taken together, the modelled global sea-level evolution is consistent with
475 reconstructions of the sea-level high stand during the LIG, but no evidence is found for sea-
476 level variations on a millennial to multi-millennial time scale that could explain a multi-peak
477 time evolution. Ice-climate feedbacks and in particular the treatment of albedo changes at the
478 atmosphere-ice sheet interface play an important role for the Greenland ice sheet. Large
479 uncertainties in the projected sea-level changes remain due to a lack of comprehensive
480 knowledge about the climate forcing at the time and a lack of constraints on LIG ice sheet
481 extent, which are limited for Greenland and virtually absent for Antarctica.

482

483 **7 Acknowledgements**

484 We acknowledge support through the Belgian Federal Science Policy Office within its
485 Research Programme on Science for a Sustainable Development under contract SD/CS/06A
486 (iCLIPS). Computational resources have been provided by the supercomputing facilities of
487 the Université catholique de Louvain (CISM/UCL) and the Consortium des Equipements de
488 Calcul Intensif en Fédération Wallonie Bruxelles (CECI) funded by the Fond de la Recherche
489 Scientifique de Belgique (FRS-FNRS).

490

491

492 **Appendix A: Ice-climate coupling improvements**

493 Compared to earlier versions of the model (Goosse et al., 2010), recent model improvements
494 for the coupling interface between climate and ice sheets have been included for the present
495 study. Ocean temperatures surrounding the Antarctic ice sheet are now used directly to
496 parameterise spatially explicit sub-ice-shelf melt rates, defining the flux boundary condition at
497 the lower surface of the Antarctic ice sheet in contact with the ocean. The sub-shelf basal melt



498 rate M_{shelf} is parameterised as a function of local mid-depth (485-700 m) ocean-water
499 temperature T_{oc} above the freezing point T_f (Beckmann and Goosse, 2003):

$$500 \quad M_{shelf} = \rho_w c_p \gamma_T F_{melt} (T_{oc} - T_f) / L \rho_i,$$

501 where $\rho_i = 910 \text{ kg m}^{-3}$ and $\rho_w = 1028 \text{ kg m}^{-3}$ are ice and seawater densities, $c_p = 3974 \text{ J kg}^{-1} \text{ }^\circ\text{C}^{-1}$
502 γ_T is the specific heat capacity of ocean water, $\gamma_T = 10^{-4}$ is the thermal exchange velocity and
503 $L = 3.35 \times 10^5 \text{ J kg}^{-1}$ is the latent heat of fusion. The local freezing point is given (Beckmann
504 and Goosse, 2003) as

$$505 \quad T_f = 0.0939 - 0.057 \cdot S_0 + 7.64 \times 10^{-4} z_b,$$

506 with a mean value of ocean salinity $S_0 = 35$ psu and the bottom of the ice shelf below sea level
507 z_b . A distinction is made between protected ice shelves (Ross and Ronne-Filchner) with a
508 melt factor of $F_{melt} = 1.6 \times 10^{-3} \text{ m s}^{-1}$ and all other ice shelves with a melt factor of $F_{melt} =$
509 $7.4 \times 10^{-3} \text{ m s}^{-1}$. The parameters are chosen to reproduce observed average melt rates (Depoorter
510 et al., 2013) under the Ross, Ronne-Filchner and Amery ice shelves for the pre-industrial
511 LOVECLIM ocean temperature and Bedmap2 (Fretwell et al., 2013) shelf geometry. For ice
512 shelves located inland from the fixed land-sea mask of the ocean model, mid-depth ocean
513 temperature from the nearest deep-ocean grid point in the same embayment is used for the
514 parameterisation.

515 In addition, surface melting of the Antarctic ice shelves has been taken into account,
516 compared to earlier model versions where all surface meltwater was assumed to refreeze at
517 the end of summer. The surface mass balance of ice sheet and ice shelf are now treated
518 consistently with the same positive-degree-day model including capillary water and refreezing
519 terms. The same melting schemes for basal and surface melt have been used for the Antarctic
520 ice sheet model version that participated in the PlioMIP intercomparison exercise of de Boer
521 et al. (2015).

522 The atmospheric interface for the Greenland ice sheet was redesigned to enable ice sheet
523 regrowth from a (semi-) deglaciated state given favourable conditions. This is accomplished
524 by preventing tundra warming affecting proximal ice sheet margins by calculating surface
525 temperatures independently for different surface types (ocean, ice sheet, tundra). At the same
526 time, the full range of atmospheric forcing is taken into account by allowing the ice sheet



527 forcing temperature to exceed the melting point at the surface. This provides an in principle
528 unbounded temperature anomaly forcing for increasing atmospheric heat content for the
529 positive-degree-day melt scheme.

530

531 **8 References**

532 Bamber, J. L., Griggs, J. A., Hurkmans, R. T. W. L., Dowdeswell, J. A., Gogineni, S. P.,
533 Howat, I., Mouginot, J., Paden, J., Palmer, S., Rignot, E., and Steinhage, D.: A new bed
534 elevation dataset for Greenland, *Cryosphere*, 7, 499-510, doi:10.5194/tc-7-499-2013, 2013.

535 Beckmann, A., and Goosse, H.: A parameterization of ice shelf-ocean interaction for climate
536 models, *Ocean Modell.*, 5, 157-170, doi:10.1016/S1463-5003(02)00019-7, 2003.

537 Berger, A.: Long-term variations of daily insolation and Quaternary climatic changes, *Journal*
538 *of Atmospheric Sciences*, 35, 2362-2367, doi:10.1175/1520-
539 0469(1978)035<2362:LTVODI>2.0.CO;2, 1978.

540 Bianchi, C., and Gersonde, R.: The Southern Ocean surface between Marine Isotope Stages 6
541 and 5d: Shape and timing of climate changes, *Palaeogeography, Palaeoclimatology,*
542 *Palaeoecology*, 187, 151-177, doi:10.1016/S0031-0182(02)00516-3, 2002.

543 Born, A., and Nisancioglu, K. H.: Melting of Northern Greenland during the last
544 interglaciation, *Cryosphere*, 6, 1239-1250, doi:10.5194/tc-6-1239-2012, 2012.

545 Clark, P., Marshall, S., Clarke, G., Hostetler, S., Licciardi, J., and Teller, J.: Freshwater
546 forcing of abrupt climate change during the last glaciation, *Science*, 293, 283-287,
547 doi:10.1126/science.1062517, 2001.

548 CLIMAP project members: Seasonal reconstruction of the earth's surface at the last glacial
549 maximum, *Geol.Soc.Am.Map Chart Ser.*, MC-36, 1981.

550 Colville, E. J., Carlson, A. E., Beard, B. L., Hatfield, R. G., Stoner, J. S., Reyes, A. V., and
551 Ullman, D. J.: Sr-Nd-Pb Isotope Evidence for Ice-Sheet Presence on Southern Greenland
552 During the Last Interglacial, *Science*, 333, 620-623, doi:10.1126/science.1204673, 2011.

553 Dansgaard, W., Clausen, H. B., Gundestrup, N., Hammer, C. U., Johnsen, S. F., Kristinsdottir,
554 P. M., and Reeh, N.: A New Greenland Deep Ice Core, *Science*, 218, 1273-1277, 1982.



- 555 de Boer, B., van de Wal, R. S. W., Lourens, L. J., Bintanja, R., and Reerink, T. J.: A
556 continuous simulation of global ice volume over the past 1 million years with 3-D ice-sheet
557 models, *Clim. Dyn.*, 41, 1365-1384, doi:10.1007/s00382-012-1562-2, 2013.
- 558 de Boer, B., Stocchi, P., and van de Wal, R. S. W.: A fully coupled 3-D ice-sheet-sea-level
559 model: algorithm and applications, *Geosci. Model Dev.*, 7, 2141-2156, doi:10.5194/gmd-7-
560 2141-2014, 2014.
- 561 de Boer, B., Dolan, A. M., Bernales, J., Gasson, E., Goelzer, H., Golledge, N. R., Sutter, J.,
562 Huybrechts, P., Lohmann, G., Rogozhina, I., Abe-Ouchi, A., Saito, F., and Van De Wal, R. S.
563 W.: Simulating the Antarctic ice sheet in the late-Pliocene warm period: PLISMIP-ANT, an
564 ice-sheet model intercomparison project, *The Cryosphere*, 9, 881-903, doi:10.5194/tc-9-881-
565 2015, 2015.
- 566 Depoorter, M. A., Bamber, J. L., Griggs, J. A., Lenaerts, J. T. M., Ligtenberg, S. R. M., van
567 den Broeke, M. R., and Moholdt, G.: Calving fluxes and basal melt rates of Antarctic ice
568 shelves, *Nature*, 502, 89-+, doi:10.1038/nature12567, 2013.
- 569 Driesschaert, E., Fichefet, T., Goosse, H., Huybrechts, P., Janssens, I., Mouchet, A.,
570 Munhoven, G., Brovkin, V., and Weber, S.: Modeling the influence of Greenland ice sheet
571 melting on the Atlantic meridional overturning circulation during the next millennia,
572 *Geophys. Res. Lett.*, 34, 10707, doi:10.1029/2007GL029516, 2007.
- 573 Dutton, A., Carlson, A. E., Long, A. J., Milne, G. A., Clark, P. U., DeConto, R., Horton, B.
574 P., Rahmstorf, S., and Raymo, M. E.: Sea-level rise due to polar ice-sheet mass loss during
575 past warm periods, *Science*, 349, aaa4019, 2015.
- 576 Duplessy, J. C., Roche, D. M., and Kageyama, M.: The deep ocean during the last interglacial
577 period, *Science*, 316, 89-91, doi:10.1126/science.1138582, 2007.
- 578 Dutton, A., and Lambeck, K.: Ice Volume and Sea Level During the Last Interglacial,
579 *Science*, 337, 216-219, doi:10.1126/science.1205749, 2012.
- 580 EPICA community members: Eight glacial cycles from an Antarctic ice core, *Nature*, 429,
581 623-628, doi:10.1038/Nature02599, 2004.
- 582 Fretwell, P., Pritchard, H. D., Vaughan, D. G., Bamber, J. L., Barrand, N. E., Bell, R.,
583 Bianchi, C., Bingham, R. G., Blankenship, D. D., Casassa, G., Catania, G., Callens, D.,
584 Conway, H., Cook, A. J., Corr, H. F. J., Damaske, D., Damm, V., Ferraccioli, F., Forsberg,



- 585 R., Fujita, S., Gim, Y., Gogineni, P., Griggs, J. A., Hindmarsh, R. C. A., Holmlund, P., Holt,
586 J. W., Jacobel, R. W., Jenkins, A., Jokat, W., Jordan, T., King, E. C., Kohler, J., Krabill, W.,
587 Riger-Kusk, M., Langley, K. A., Leitchenkov, G., Leuschen, C., Luyendyk, B. P., Matsuoka,
588 K., Mouginot, J., Nitsche, F. O., Nogi, Y., Nost, O. A., Popov, S. V., Rignot, E., Rippin, D.
589 M., Rivera, A., Roberts, J., Ross, N., Siegert, M. J., Smith, A. M., Steinhage, D., Studinger,
590 M., Sun, B., Tinto, B. K., Welch, B. C., Wilson, D., Young, D. A., Xiangbin, C., and
591 Zirizzotti, A.: Bedmap2: improved ice bed, surface and thickness datasets for Antarctica,
592 *Cryosphere*, 7, 375-393, doi:10.5194/tc-7-375-2013, 2013.
- 593 Goelzer, H., Huybrechts, P., Loutre, M.-F., and Fichefet, T.: Impact of ice sheet meltwater
594 fluxes on the climate evolution at the onset of the Last Interglacial, *Clim. Past. Discuss.*, 11,
595 4391-4423, doi:10.5194/cpd-11-4391-2015, 2015.
- 596 Goelzer, H., Huybrechts, P., Loutre, M. F., Goosse, H., Fichefet, T., and Mouchet, A.: Impact
597 of Greenland and Antarctic ice sheet interactions on climate sensitivity, *Clim. Dyn.*, 37, 1005-
598 1018, doi:10.1007/s00382-010-0885-0, 2011.
- 599 Goelzer, H., Huybrechts, P., Raper, S. C. B., Loutre, M. F., Goosse, H., and Fichefet, T.:
600 Millennial total sea level commitments projected with the Earth system model of intermediate
601 complexity LOVECLIM *Environ. Res. Lett.*, 7, 045401, doi:10.1088/1748-9326/7/4/045401,
602 2012.
- 603 Golledge, N. R., Menviel, L., Carter, L., Fogwill, C. J., England, M. H., Cortese, G., and
604 Levy, R. H.: Antarctic contribution to meltwater pulse 1A from reduced Southern Ocean
605 overturning, *Nature Communications*, 5, 5107, doi:10.1038/ncomms6107, 2014.
- 606 Goosse, H., Brovkin, V., Fichefet, T., Haarsma, R., Huybrechts, P., Jongma, J., Mouchet, A.,
607 Selten, F., Barriat, P.-Y., Campin, J.-M., Deleersnijder, E., Driesschaert, E., Goelzer, H.,
608 Janssens, I., Loutre, M. F., Morales Maqueda, M. A., Opsteegh, T., Mathieu, P.-P.,
609 Munhoven, G., Pettersson, E. J., Renssen, H., Roche, D. M., Schaeffer, M., Tartinville, B.,
610 Timmermann, A., and Weber, S. L.: Description of the Earth system model of intermediate
611 complexity LOVECLIM version 1.2, *Geosci. Model Dev.*, 3, 603-633, doi:10.5194/gmd-3-
612 603-2010, 2010.
- 613 Grant, K. M., Rohling, E. J., Bar-Matthews, M., Ayalon, A., Medina-Elizalde, M., Ramsey,
614 C. B., Satow, C., and Roberts, A. P.: Rapid coupling between ice volume and polar



- 615 temperature over the past 150,000 years, *Nature*, 491, 744–747, doi:10.1038/nature11593,
616 2012.
- 617 Holden, P., Edwards, N. R., Wolff, E., Lang, N., Singarayer, J., Valdes, P., and Stocker, T.:
618 Interhemispheric coupling, the West Antarctic Ice Sheet and warm Antarctic interglacials,
619 *Clim. Past.*, 6, 431–443, doi:10.5194/cp-6-431-2010, 2010.
- 620 Huybrechts, P.: Sea-level changes at the LGM from ice-dynamic reconstructions of the
621 Greenland and Antarctic ice sheets during the glacial cycles, *Quat. Sci. Rev.*, 21, 203–231,
622 doi:10.1016/S0277-3791(01)00082-8, 2002.
- 623 Huybrechts, P., and de Wolde, J.: The dynamic response of the Greenland and Antarctic ice
624 sheets to multiple-century climatic warming, *J. Clim.*, 12, 2169–2188, doi:10.1175/1520-
625 0442(1999)012<2169:TDROTG>2.0.CO;2, 1999.
- 626 Kopp, R. E., Simons, F. J., Mitrovica, J. X., Maloof, A. C., and Oppenheimer, M.:
627 Probabilistic assessment of sea level during the last interglacial stage, *Nature*, 462, 863–867,
628 doi:10.1038/nature08686, 2009.
- 629 Kopp, R. E., Simons, F. J., Mitrovica, J. X., Maloof, A. C., and Oppenheimer, M.: A
630 probabilistic assessment of sea level variations within the last interglacial stage, *Geophys. J.*
631 *Int.*, 193, 711–716, doi:10.1093/gji/ggt029, 2013.
- 632 Lisiecki, L. E., and Raymo, M. E.: A Pliocene-Pleistocene stack of 57 globally distributed
633 benthic delta O-18 records, *Paleoceanography*, 20, PA1003, doi:10.1029/2004pa001071,
634 2005.
- 635 Loutre, M. F., Fichet, T., Goosse, H., Huybrechts, P., Goelzer, H., and Capron, E.: Factors
636 controlling the last interglacial climate as simulated by LOVECLIM1.3, *Clim. Past.*, 10,
637 1541–1565, doi:10.5194/cp-10-1541-2014, 2014.
- 638 MacGregor, J. A., and Fahnstock, M. A.: Radiostratigraphy and age structure of the
639 Greenland Ice Sheet, *J Geophys Res-Earth*, 120, 212–241, doi:10.1002/2014JF003215, 2015.
- 640 Masson-Delmotte, V., Schulz, M., Abe-Ouchi, A., Beer, J., Ganopolski, A., González Rouco,
641 J., Jansen, E., Lambeck, K., Luterbacher, J., Naish, T., Osborn, T., Otto-Bliesner, B., Quinn,
642 T., Ramesh, R., Rojas, M., Shao, X., and Timmermann, A.: Information from paleoclimate
643 archives, in: *Climate Change 2013: The Physical Science Basis. Contribution of Working*
644 *Group I to the Fifth Assessment Report of the Intergovernmental Panel on Climate Change,*



- 645 edited by: Stocker, T. F., Qin, D., Plattner, G.-K., Tignor, M., Allen, S. K., Boschung, J.,
646 Nauels, A., Xia, Y., Bex, V., and Midgley, P. M., Cambridge University Press, Cambridge,
647 United Kingdom and New York, NY, USA, 383-464, 2013.
- 648 Masson-Delmotte, V., Steen-Larsen, H. C., Ortega, P., Swingedouw, D., Popp, T., Vinther, B.
649 M., Oerter, H., Sveinbjornsdottir, A. E., Gudlaugsdottir, H., Box, J. E., Falourd, S., Fettweis,
650 X., Gallee, H., Garnier, E., Gkinis, V., Jouzel, J., Landais, A., Minster, B., Paradis, N., Orsi,
651 A., Risi, C., Werner, M., and White, J. W. C.: Recent changes in north-west Greenland
652 climate documented by NEEM shallow ice core data and simulations, and implications for
653 past-temperature reconstructions, *Cryosphere*, 9, 1481-1504, doi:10.5194/tc-9-1481-2015,
654 2015.
- 655 Merz, N., Born, A., Raible, C. C., Fischer, H., and Stocker, T. F.: Dependence of Eemian
656 Greenland temperature reconstructions on the ice sheet topography, *Clim. Past*, 10, 1221-
657 1238, doi:10.5194/cp-10-1221-2014, 2014.
- 658 NEEM community members: Eemian interglacial reconstructed from a Greenland folded ice
659 core, *Nature*, 493, 489-494, doi:10.1038/nature11789, 2013.
- 660 Pollard, D., DeConto, R. M., and Alley, R. B.: Potential Antarctic Ice Sheet retreat driven by
661 hydrofracturing and ice cliff failure, *Earth Planet. Sci. Lett.*, 412, 112-121,
662 doi:10.1016/j.epsl.2014.12.035, 2015.
- 663 Robinson, A., Calov, R., and Ganopolski, A.: Greenland ice sheet model parameters
664 constrained using simulations of the Eemian Interglacial, *Clim. Past.*, 7, 381-396,
665 doi:10.5194/cp-7-381-2011, 2011.
- 666 Robinson, A., and Goelzer, H.: The importance of insolation changes for paleo ice sheet
667 modeling, *The Cryosphere*, 8, 1419-1428, doi:10.5194/tc-8-1419-2014, 2014.
- 668 Rohling, E. J., Foster, G. L., Grant, K. M., Marino, G., Roberts, A. P., Tamisiea, M. E., and
669 Williams, F.: Sea-level and deep-sea-temperature variability over the past 5.3 million years,
670 *Nature*, 508, 477-482, doi:10.1038/nature13230, 2014.
- 671 Rybak, O., and Huybrechts, P.: The configuration of the Greenland ice sheet during the last
672 Interglacial constrained by ice-core data, to be submitted.



- 673 Shakun, J. D., Lea, D. W., Lisiecki, L. E., and Raymo, M. E.: An 800-kyr record of global
674 surface ocean delta O-18 and implications for ice volume-temperature coupling, *Earth Planet.
675 Sci. Lett.*, 426, 58-68, doi:10.1016/j.epsl.2015.05.042, 2015.
- 676 Sjolte, J., and Hoffmann, G.: Modelling stable water isotopes in monsoon precipitation during
677 the previous interglacial, *Quat. Sci. Rev.*, 85, 119-135, doi:10.1016/j.quascirev.2013.12.006,
678 2014.
- 679 Steen-Larsen, H. C., Masson-Delmotte, V., Hirabayashi, M., Winkler, R., Satow, K., Prié, F.,
680 Bayou, N., Brun, E., Cuffey, K. M., Dahl-Jensen, D., Dumont, M., Guillevic, M., Kipfstuhl,
681 S., Landais, A., Popp, T., Risi, C., Steffen, K., Stenni, B., and Sveinbjörnsdóttir, A. E.: What
682 controls the isotopic composition of Greenland surface snow?, *Clim. Past.*, 10, 377-392,
683 doi:10.5194/cp-10-377-2014, 2014.
- 684 Steig, E. J., Huybers, K., Singh, H. A., Steiger, N. J., Ding, Q. H., Frierson, D. M. W., Popp,
685 T., and White, J. W. C.: Influence of West Antarctic Ice Sheet collapse on Antarctic surface
686 climate, *Geophys. Res. Lett.*, 42, 4862-4868, doi:10.1002/2015GL063861, 2015.
- 687 Stone, E. J., Lunt, D. J., Annan, J. D., and Hargreaves, J. C.: Quantification of the Greenland
688 ice sheet contribution to Last Interglacial sea level rise, *Clim. Past.*, 9, 621-639,
689 doi:10.5194/cp-9-621-2013, 2013.
- 690 Swingedouw, D., Fichet, T., Huybrechts, P., Goosse, H., Driesschaert, E., and Loutre, M.
691 F.: Antarctic ice-sheet melting provides negative feedbacks on future climate warming,
692 *Geophys. Res. Lett.*, 35, L17705, doi:10.1029/2008GL034410, 2008.
- 693 Thompson, W. G., Curran, H. A., Wilson, M. A., and White, B.: Sea-level oscillations during
694 the last interglacial highstand recorded by Bahamas corals, *Nat. Geosci.*, 4, 684-687,
695 doi:10.1038/ngeo1253, 2011.
- 696 Turney, C. S. M., and Jones, R. T.: Does the Agulhas Current amplify global temperatures
697 during super-interglacials?, *J. Quat. Sci.*, 25, 839-843, doi:10.1002/jqs.1423, 2010.
- 698 van de Berg, W. J., van den Broeke, M. R., van Meijgaard, E., and Kaspar, F.: Importance of
699 precipitation seasonality for the interpretation of Eemian ice core isotope records from
700 Greenland, *Clim. Past.*, 9, 1589-1600, doi:10.5194/cp-9-1589-2013, 2013.

701

702



703 **9 Tables**

704 **Table 1 Peak sea-level contribution and timing from the Greenland ice sheets above present-day levels for**
705 **three different parameter choices.**

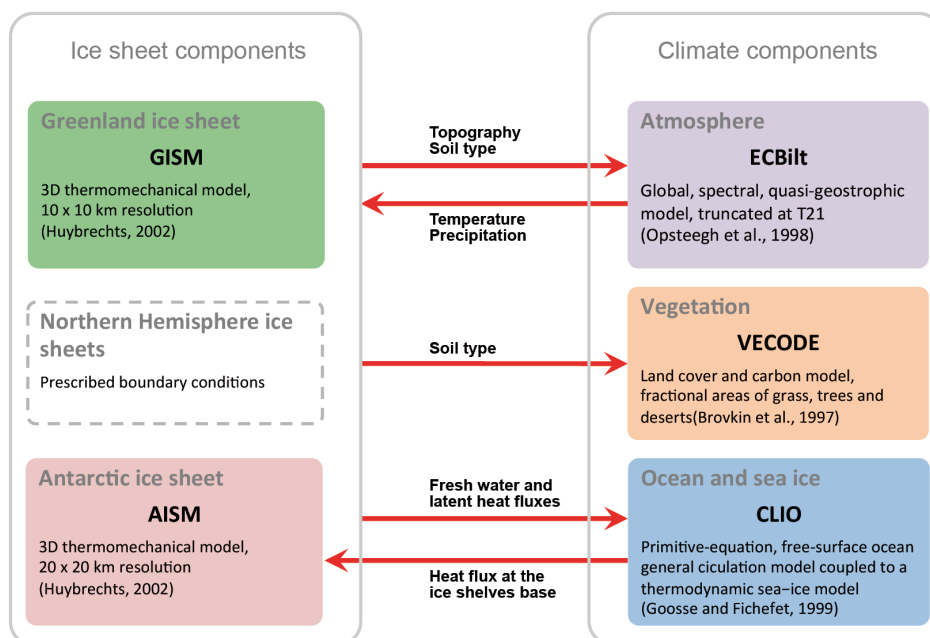
	Fully coupled experiments		Stand-alone repeat experiments	
EXP	SLE (m)	time of peak	SLE (m)	time of peak
high	2.77	-122.5	2.02	-123.3
reference	1.42	-123.0	1.42	-123.0
low	0.62	-123.8	0.83	-123.3

706

707



708 **10 Figures**

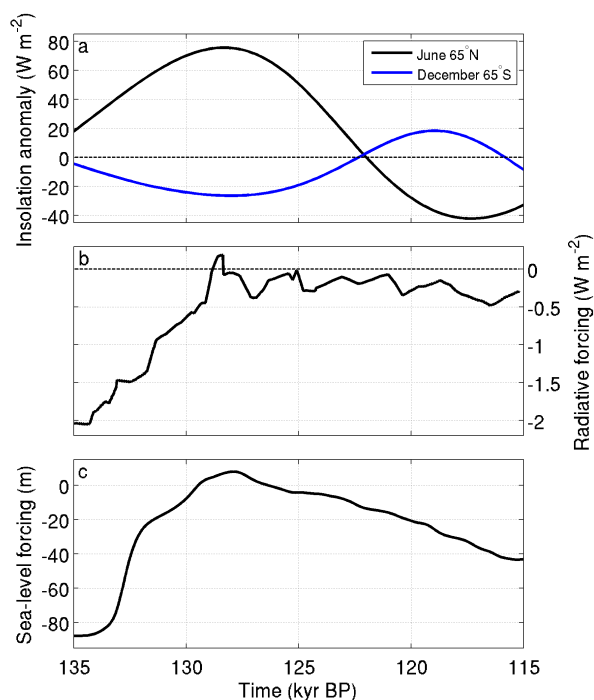


709

710 **Figure 1 LOVECLIM model setup for the present study including dynamic components for the Greenland**
711 **and Antarctic ice sheets and prescribed Northern Hemisphere ice sheet boundary conditions.**

712

713

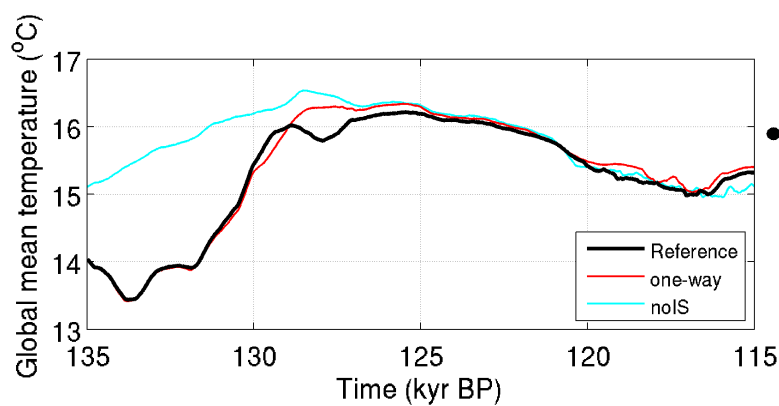


714

715 **Figure 2: Prescribed model forcing. Top: average monthly insolation anomaly at 65° North in June**
716 **(black) and 65° South in December (blue). Middle: combined radiative forcing anomaly of prescribed**
717 **greenhouse gas concentrations relative to the present day. Bottom: sea-level forcing for the ice sheet**
718 **components derived from a Red Sea sea-level record (Grant et al. 2012).**

719

720



721

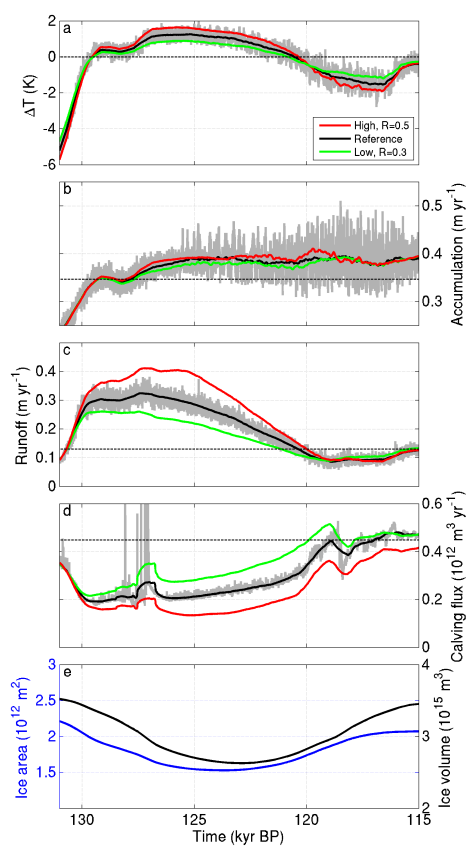
722 **Figure 3: Global annual mean near-surface air temperature evolution of the reference run (black)**
723 **compared to experiments with prescribed Greenland and Antarctic ice sheet evolution from stand-alone**
724 **experiments (one-way, red) and no ice sheet changes at all (noIS, light blue). The filled circle on the right**
725 **axis indicates the temperature for a pre-industrial control experiment of the reference model with present**
726 **day ice sheet configuration.**

727

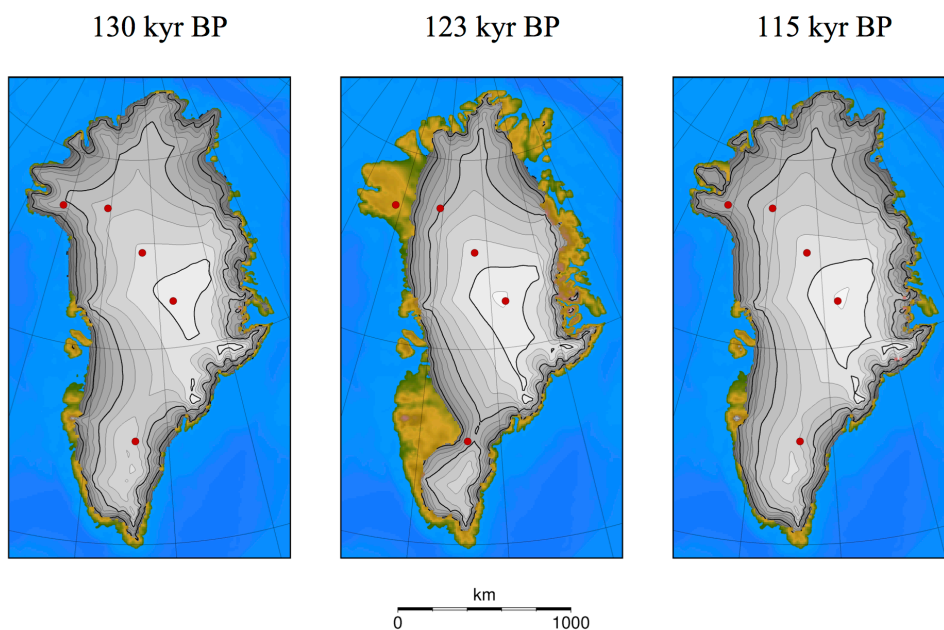
728



729



730 **Figure 4** Greenland ice sheet forcing characteristics for the reference run (black) and with higher (red)
731 and lower (green) temperature scaling. Climatic temperature anomaly relative to pre-industrial (a),
732 accumulation rate (b) and runoff rate (c) are given as ice sheet wide spatial averages over grounded ice.
733 Calving flux (d) and other mass balance terms (b, c) are given in water equivalent. (e) Ice area (blue) and
734 ice volume (black) for the reference run. All lines are smoothed with a 400 years running mean except for
735 the grey lines giving the full annual time resolution for the reference run.
736



737

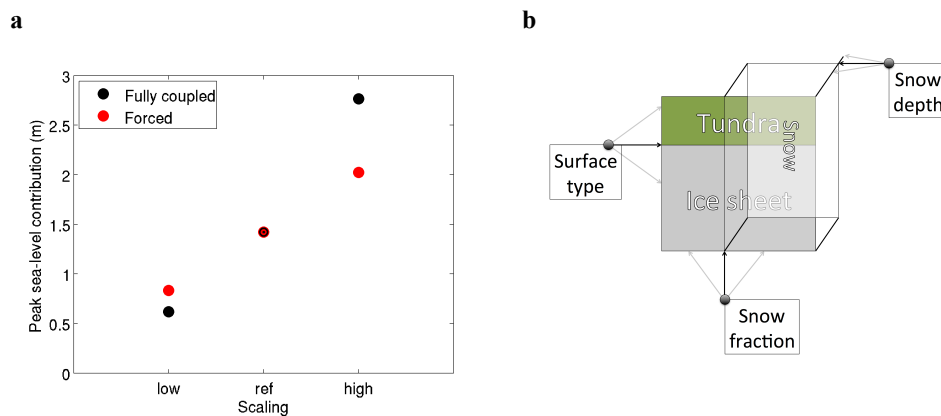
738 **Figure 5 Greenland ice sheet geometry at 130 kyr BP (left), for the minimum ice sheet volume at 123 kyr**
739 **BP with a SL contribution of 1.4 m (middle) and at the end of the reference experiment at 115 kyr BP**
740 **(right). The red dots indicate the deep ice core locations (from south to northwest: Dye-3, GRIP, NGRIP,**
741 **NEEM, Camp Century).**

742

743



744



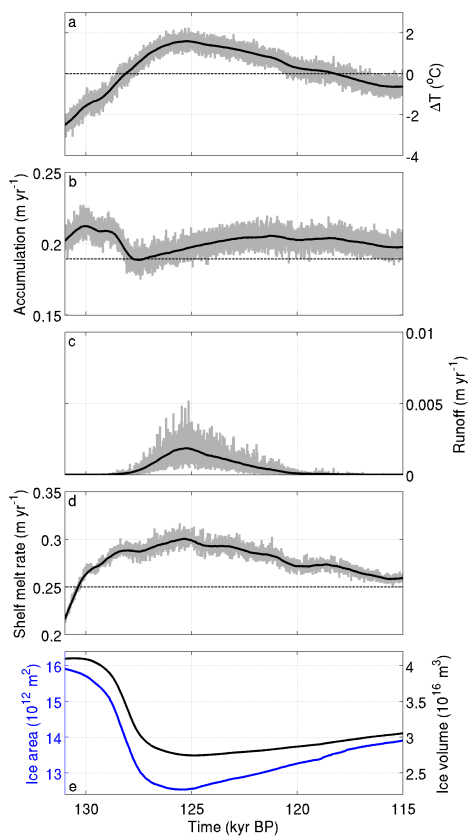
745 **Figure 6 (a) Scaling of sea-level contribution from the Greenland ice sheet as a function of temperature**
746 **changes for the full model (black) and forced model (red) in comparison. (b) Schematic of the albedo**
747 **parameterisation in the land model for (partially) ice-covered areas.**

748

749



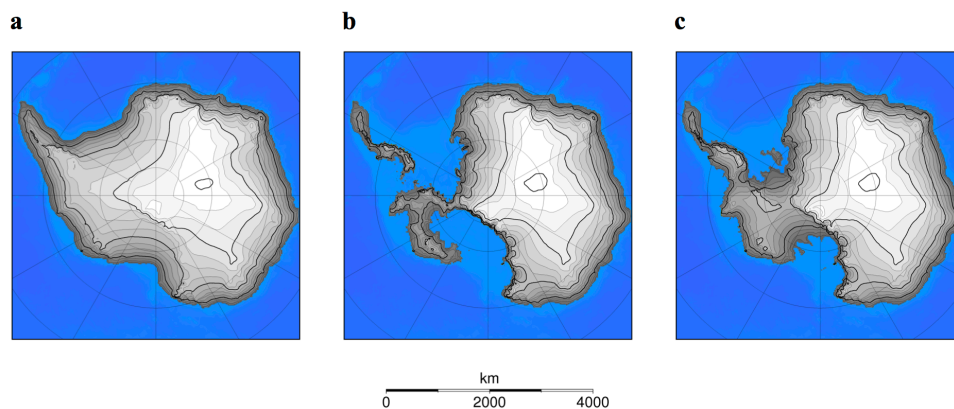
750



751 **Figure 7 Antarctic ice sheet forcing and characteristics. Temperature anomaly relative to pre-industrial**
752 **(a), average ice sheet wide accumulation rate (b), average ice sheet wide runoff rate (c), average shelf melt**
753 **rate diagnosed for the area of the present-day observed ice shelves (d). (e) Grounded ice sheet area (blue)**
754 **and volume (black). Grey lines give full annual time resolution, while black lines (and blue in e) are**
755 **smoothed with a 400 years running mean.**

756

757



758

759

760

761

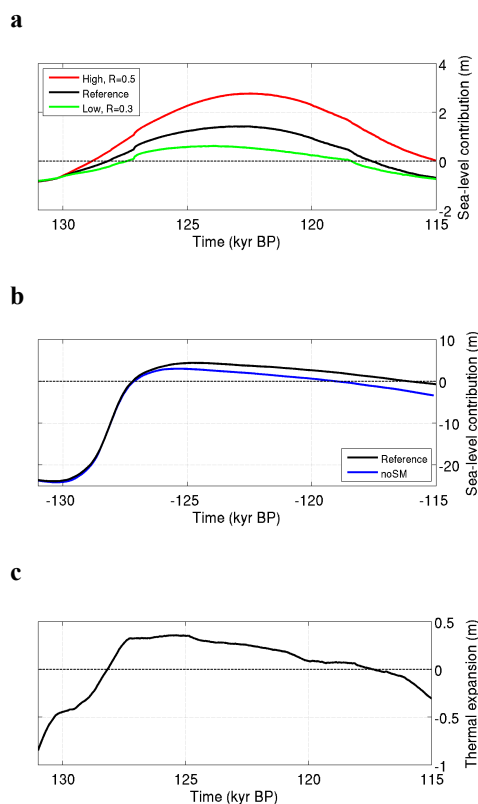
762

763

Figure 8 Antarctic grounded ice sheet geometry at 130 kyr BP (a), for the minimum ice sheet volume at 125 kyr BP with a SL contribution of 4.4 m (b) and at the end of the reference experiment at 115 kyr BP (c).



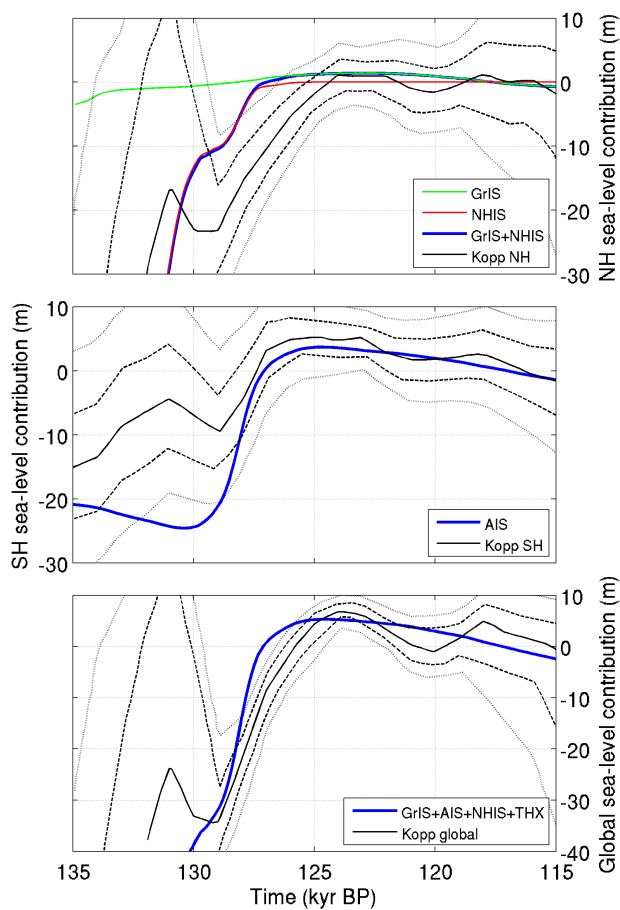
764



765 **Figure 9 (a) Sea-level contribution from the Greenland ice sheet for the reference run (black) and two**
766 **sensitivity experiments with higher (red) and lower (green) temperature scaling. (b) Sea-level contribution**
767 **from the Antarctic ice sheet from the reference run (black) and from a sensitivity experiment without**
768 **shelf melting (blue). (c) Sea-level contribution from oceanic thermal expansion from the reference run.**

769

770



771

772 **Figure 10** Modelled sea-level contributions from this study (colour lines) compared to probabilistic sea-
773 level reconstructions (black lines) from Kopp et al. (2009).

774